PHYSICAL REVIEW B **94**, 180103(R) (2016)

Microscopic origin of entropy-driven polymorphism in hybrid organic-inorganic perovskite materials

Keith T. Butler,[1,*] Katrine Svane,[1] Gregor Kieslich,[2,3,†] Anthony K. Cheetham,[2] and Aron Walsh[4]

[1]*Department of Chemistry, University of Bath, Claverton Down, Bath BA2 7AY, United Kingdom*

[2]*Department of Materials Science and Metallurgy, University of Cambridge, Cambridge CB3 0FS, United Kingdom*

[3]*Department of Chemistry, Technical University of Munich, Department of Chemistry, Lichtenbergstraße 4, Munich, Germany*

[4]*Department of Materials, Imperial College London, Royal School of Mines, Exhibition Road, London SW7 2AZ, United Kingdom*

(Received 26 August 2016; published 7 November 2016)

Entropy is a critical, but often overlooked, factor in determining the relative stabilities of crystal phases. The importance of entropy is most pronounced in softer materials, where small changes in free energy can drive phase transitions, which has recently been demonstrated in the case of organic-inorganic hybrid-formate perovskites. In this Rapid Communication we demonstrate the interplay between composition and crystal structure that is responsible for the particularly pronounced role of entropy in determining polymorphism in hybrid organic-inorganic materials. Using *ab initio* based lattice dynamics, we probe the origins and effects of vibrational entropy of four archetype perovskite (ABX_3) structures. We consider an inorganic material ($SrTiO_3$), an *A*-site hybrid-halide material $(CH_3NH_3)PbI_3$, a *X*-site hybrid material $KSr(BH_4)_3$, and a mixed *A*- and *X*-site hybrid-formate material $(N_2H_5)Zn(HCO_2)_3$, comparing the differences in entropy between two common polymorphs. The results demonstrate the importance of low-frequency intermolecular modes in determining the phase stability in these materials. The understanding gained allows us to propose a general principle for the relative stability of different polymorphs of hybrid materials as temperature is increased.

DOI: 10.1103/PhysRevB.94.180103

The interplay between structure and function is the cornerstone of modern materials design. The ability to rationally predict and control how composition affects structure and how, together, they determine materials properties is at the heart of this pursuit. Since the early 20th century scientists have developed a host of models to describe how simple elemental properties determine crystal structure. The pioneering work of Goldschmidt—predicting perovskite structures based on radius ratios [1]—and Pauling—elucidating the roles of bond valence and electronegativity [2]—stand as some of the most important works in the field of materials design. Other notable successes include the Goodenough-Kanamori rules [3,4], the hard-soft acid/base classification [5], and of intermetallic alloy formation maps [6]. Recently, density functional theory (DFT) has become a powerful tool for assisting materials design [7–9]. The rise of quantitatively predictive computational techniques has led to a proliferation of data—the Materials Project [10] now contains accurate calculated data on over 60 000 known materials. With this wealth of data, the role of simple rules and descriptors to relate composition to function is more important than ever [11].

The success stories outlined above have all been achieved in the field of purely inorganic materials, but today the specter of hybrid organic-inorganic systems looms large. These are materials with a well-defined crystal structure, where at least one Wyckoff site is occupied by a molecular species. These materials rose to prominence, driven largely by the success of metal-organic frameworks (MOFs) [12,13]. In recent years they have become increasingly of interest in fields such as multiferroics [14,15] and electronics [16]; notably, the hybrid-perovskite materials have revolutionized the field of photovoltaics [17–20].

Despite numerous studies of hybrid materials' properties [21–24], design principles, such as those reported for inorganic materials, are few and far between [25,26]. Generally, in inorganic solids, the favorable polymorph is that which is enthalpically most stable; statistical and entropic effects are recognized as a major factor for other phase transitions, such as those in $SrTiO_3$ [27], and $BaTiO_3$ [28–31].

There is an almost endless number of possible contributions to the entropy of a system, from compositional, structural, magnetic, etc., sources [32]. It would be impossible to define an absolute contribution from entropy to the stability of a phase; however, it is possible to identify and quantify the most important contributions. In solid state systems and, in particular, hybrid organic-inorganic systems, the most important contributions will be from configurational, rotational, and vibrational entropy. Theoretical calculations make it possible to evaluate each of these contributions individually, elucidating their importance (or lack thereof) in determining crystal structure, which in turn allows for the development of experimental strategies to exploit this dependence to direct synthetic efforts.

The role of rotational entropy has been recognized in hybrid-perovskite materials [33,34]; based on accessible orientational microstates, rotational entropy in the region of $R\ln(3)$–$R\ln(8)$, corresponding to 5.8–17.3 J K^{-1} mol^{-1}, is predicted [33,34]. Configurational entropy is recognized as an important contribution in many systems, determining the probability of mixing in both organic [35] and inorganic alloys [36]. Lattice dynamics has been applied to demonstrate how vibrational entropy can play a critical role in determining the stable polymorph of hybrid materials [37–39], and the role of molecule-cavity interactions, determining the

*k.t.butler@bath.ac.uk

†Gregor.Kieslich@tum.de

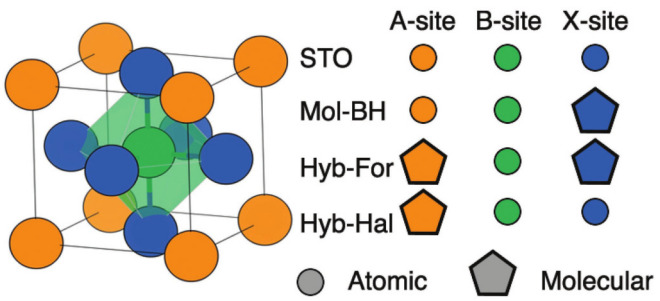

FIG. 1. The crystal composition of the perovskite materials with various molecular components studied, demonstrating different types of hybrids. STO ($SrTiO_3$), Mol-BH [$KSr(BH_4)_3$], Hyb-For $(N_2H_5)Zn(HCO_2)_3$, and Hyb-Hal $(CH_3NH_3)PbI_3$.

mechanical properties of the formate perovskites, has also been recognized [40].

In this Rapid Communication we probe the basis of the vibrational entropy, which can drive polymorphism in hybrid-perovskite materials. By isolating the contributions from vibrational entropy alone we are able to demonstrate that it plays an important role in determining the thermodynamic balance between the phases of each of the hybrid materials that we consider. We are able to quantify this contribution and, moreover, to identify a microscopic mechanism responsible for these observations. We demonstrate the generality of the importance of vibrational entropy in hybrid organic-inorganic materials, a finding which was only reported in a select few specific systems to date.

We study the materials pictured schematically in Fig. 1, comprising frameworks of corner-sharing BX_3 octahedral units, with A sites occupying the cavity. We consider $SrTiO_3$ (STO), $(CH_3NH_3)PbI_3$ (Hyb-Hal), $KSr(BH_4)_3$ (Mol-BH_4), and $(N_2H_5)Zn(HCO_2)_3$ (Hyb-For), comparing the differences in entropy between two common polymorphs. STO is studied in its room-temperature (cubic) and low-temperature (tetragonal) structures. Hyb-Hal is considered in its high-temperature (pseudocubic) and room-temperature (tetragonal) phases [41]—these vibrational spectra were calculated as part of a previous study [42]. Hyb-For is studied in its experimentally reported polymorphs, perovskite ($Pna2_1$) and the channel structure ($P2_12_12_1$) [37]. Mol-BH_4 is studied in the experimentally determined orthorhombic structure [43], which we have also found to be the most stable phase, and a pseudocubic structure.

The free energy of the system is calculated within the quasiharmonic approximation from

$$G(T,p) = \min_V [U(V) + F_{\rm ph}(T;V) + pV], \qquad (1)$$

where the the internal energy of the system as a function of volume $U(V)$ is obtained from DFT calculations. The phonon free energy ($F_{\rm ph}$) arising from harmonic vibrations of the lattice is calculated within the frozen phonon approximation. The effect of thermal expansion of the lattice is approximated by considering the energy-volume relationship. The underlying vibrational entropy is calculated from the phonon density of states of all positive phonon modes according to

$$S_{\rm vib}(T) = 3k_B \int_0^\infty g(\varepsilon)\{[n(\varepsilon)+1]\ln[n(\varepsilon)+1] - n(\varepsilon)\ln[n(\varepsilon)]\}d\varepsilon, \qquad (2)$$

where k_B is the Boltzmann constant, $g(\varepsilon)$ is the normalized phonon density of states with energy ε, $n(\varepsilon)$ is the Bose-Einstein population of a state of energy ε at temperature T, and $\varepsilon = \hbar\omega$, where ω is the mode frequency. The energies and forces of the systems are calculated from DFT, using the PBEsol functional [44] in the VASP package [45] within the projector augmented wave formalism [46]. We use a cutoff energy of 500 eV and a k-point mesh sampling density with a target length cutoff of 25 Å, as prescribed by Moreno and Soler [47]. The dynamical matrix and phonon frequencies are obtained using the PHONOPY package [48].

The difference in vibrational entropy between the polymorphs of STO is significantly lower than in the hybrid systems (see Fig. 2). This implies that vibrational entropy plays little role in determining the relative stabilities of different phases of this purely inorganic perovskite in the temperature range considered here; configurational entropy is generally more relevant in these materials.

The vibrational entropies of the two polymorphs of all three hybrid materials evolve differently with temperature, resulting in significant differences in $S_{\rm vib}$ at 300 K—ΔS of the order of 10–100 J K^{-1} mol^{-1}, at least as large as the rotational entropy and sufficient to shift equilibrium in the synthesis of formate perovskites [37]. In all three hybrid materials studied here we find that the order of thermodynamic stability of the polymorphs is reversed as the temperature is increased (see Fig. 2). The presence of a discrete molecular unit at the A or X site is an important factor in determining the differences in

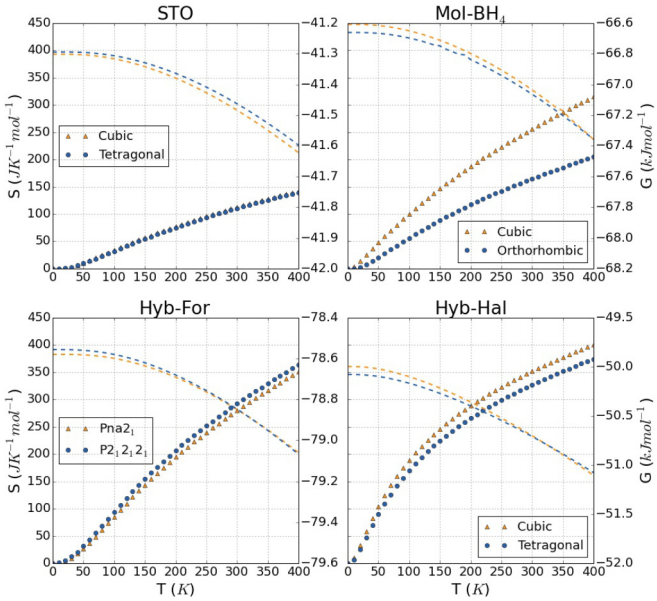

FIG. 2. The vibrational entropy [calculated from Eq. (1); markers] and Gibbs free energy (dashed lines) for two phases of each of the materials studied across a temperature range. Calculations were performed within the quasiharmonic approximation.

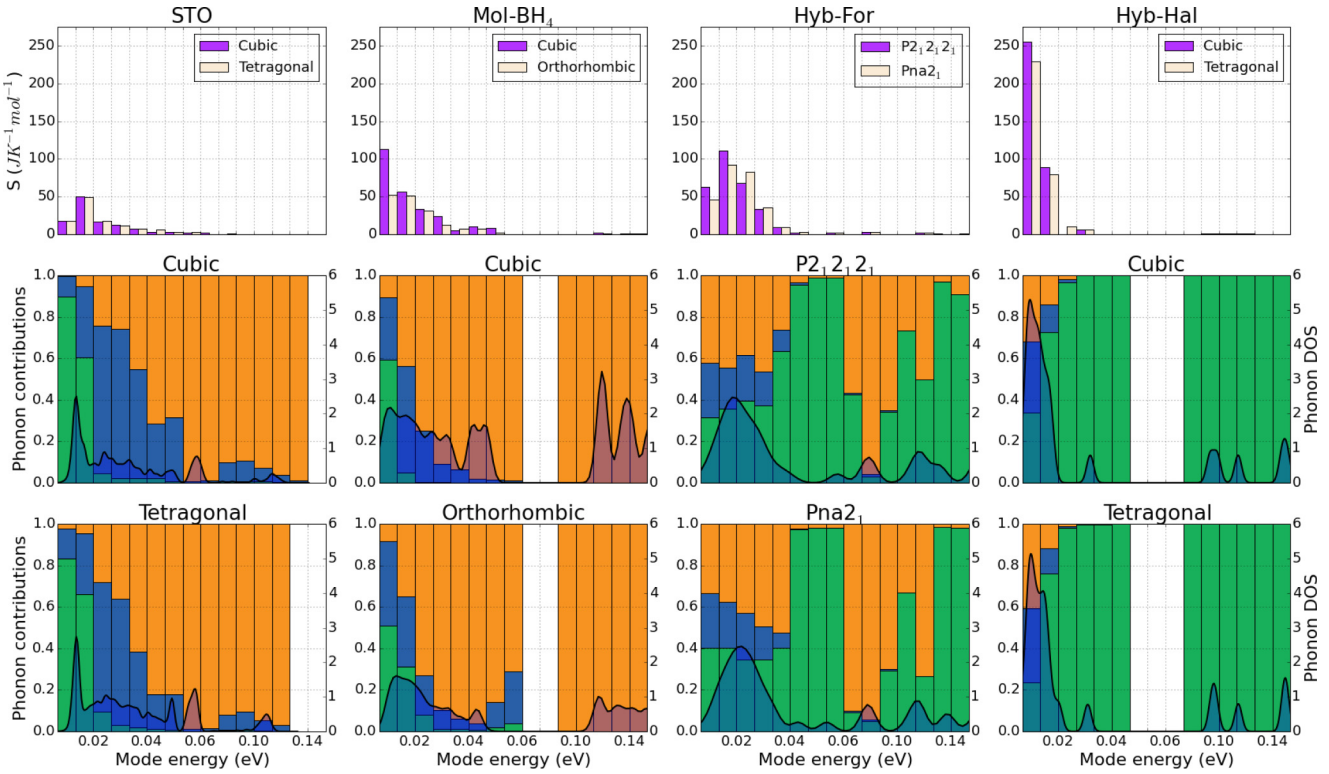

FIG. 3. Decomposition of contributions to vibrational entropy for the four compositions studied. Each column is plotted on a common abscissa, where the phonon modes are separated into bins of 0.1 eV. Upper row: The vibrational entropy of both phases decomposed by energy; each 0.1 interval features the entropy of both of the phases studies. Middle and lower rows: The fractional contribution of each crystal site to the total vibrational entropy within the corresponding energy range; *A* site (green), *B* site (blue), *X* site (yellow). The phonon density of states for each polymorph is superimposed on the contribution plot.

the vibrational entropies between phases of hybrid-perovskite materials. In order to further analyze this, we deconvolute the phonon contributions to vibrational entropy.

The contributions of the low-frequency phonon modes to vibrational entropy of the different phases are compared in the top row of Fig. 3 (in the Supplemental Material [49] we demonstrate that only modes up to 0.04 eV contribute significantly to vibrational entropy at the temperatures considered). The STO vibrational entropy contribution is significantly lower than that found in the other materials. In all three hybrid materials there are differences between the vibrational entropies in the various regions of the phonon density of states, but most notably at the low frequency end of the spectrum. This explains why the hybrid materials have vibrational entropy differences between polymorphs large enough to determine a relative phase stability close to room temperature, while STO does not.

To probe the atomistic origins of the above observation, we have decomposed the contributions to the phonon spectrum by the crystal site (see Fig. 3). We calculate $\langle g_i(\varepsilon)\rangle$, the weighted average of the phonon density of states of a given site i at energy ε,

$$\langle g_i(\varepsilon)\rangle = \frac{\sum_j w_{ij}}{\sum_k w_k}, \tag{3}$$

where w_{ij} are the weights of the phonon modes (w_j) involving the site i at energy ε and w_k are all phonon mode weights at energy ε—we note that the phonon mode weights account for the mass of the ions involved in the modes.

In STO the decomposed density of states (DOS) are almost identical for each phase, consistent with the finding (Fig. 2) that the vibrational entropies are indistinguishable in this material. In all three hybrid materials the lower end of the phonon spectrum is evenly distributed between the *A* site and the framework, indicative of a collective of phonon modes, which arise from interactions between the framework and the *A* site. In the hybrid materials the differences in vibrational entropy between polymorphs, which can determine the balance of thermodynamic stability, are determined by changes in the vibrations in this lower part of the spectrum.

The smaller number of states at low-frequency in STO corresponds to the absence of soft intermolecular bonding in the inorganic material, where the majority of the bonding is of the strong ionic or covalent type. These bonds are typically much stiffer than intermolecular bonds and have higher vibrational frequencies. In the hybrid systems, each material has a range of soft intermolecular forces, notably hydrogen bonds, which result in a high DOS at the low end of the phonon energy spectrum.

In order to provide a more quantitative measure of the effects of chemical bonding, the degree of vibrational entropy associated with an atomic site can be conveniently expressed by the thermal ellipsoid or atomic displacement parameter (ADP). The ADP provides a Boltzmann averaged measure of the vibrational disorder. The volume of the ellipsoid is determined by the probability of finding the electronic density associated with a given site within the boundaries; it is common

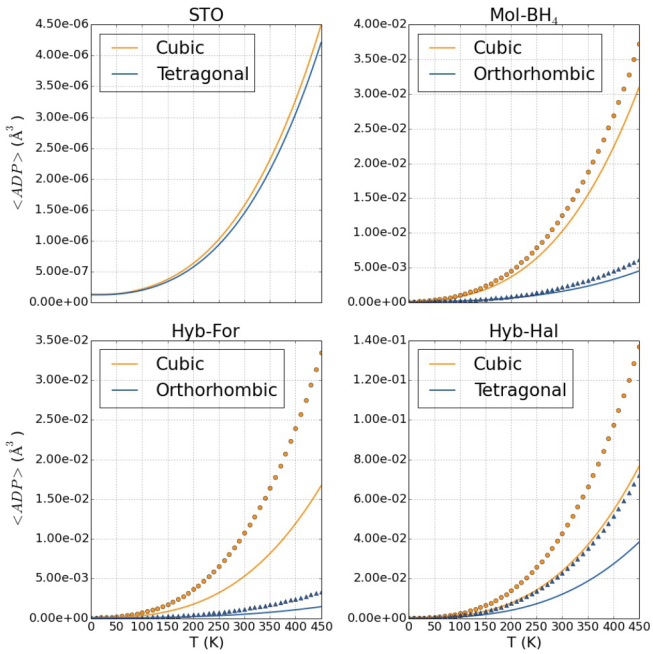

FIG. 4. The evolution of atomic displacement volumes with temperature. The anisotropic factor B, calculated as in Eq. (4), is used to calculate the volume, which is plotted for each polymorph across the temperature range 0–450 K. Total mean ADP volumes for all atoms are represented by a line, and hydrogen only mean ADP volumes are represented by markers.

to apply a probability of 50%. In order to compare the atomic site contributions to the vibrational entropy, we can therefore compare the ADPs (here the B value), which are obtained from the phonon spectrum according to

$$B(j) = \frac{\hbar}{2Nm_j} \sum_{q,v} \omega_v(q)^{-1}[1 + 2n_v(q)]e_v(j,q) \times e_v^*(j,q), \tag{4}$$

where N is the number of unit cells, m_j is the atomic mass, $\omega_v(q)$ is the frequency, e_v is the polarization vector, and n_v is the thermal population of the band.

The evolution of the mean ADPs with temperature is plotted in Fig. 4, together with the evolution of the mean volume of the hydrogen ADPs (where they are present). The plot shows that in cases where there is a significant difference between the mean ADPs of different polymorphs, the difference arises from the hydrogen based ADPs. In STO, where there are no hydrogens, the ADPs of both polymorphs evolve identically. In all of the hybrid materials, the mean ADPs evolve in the same way as the vibrational entropy, and the difference between ADPs of the polymorphs is due, almost entirely, to differences between the hydrogen ADPs.

In all three hybrid materials, the higher-temperature polymorph is the one with the larger cavity size, either cubic or hexagonal channels (in the Hyb-For). The high-temperature polymorph can thereby maximize the number of weak intermolecular forces (predominantly H bonds) and hence increase the low frequency DOS. Hyb-For demonstrates this subtle interplay of enthalpy and entropy exquisitely. In the $Pna2_1$ phase the phonon DOS has a peak at a higher frequency than the $P2_12_12_1$ phase. The higher frequency peak reflects slightly stiffer interatomic bonding, related to salt-bridge-like interactions between the molecular A-site cation $NH_3NH_2^+$ and the pseudocubic cavity. The total free energy also contains a contribution from vibrational entropy. As the temperature rises, the latter contribution begins to outweigh the former and the phase with softer, more flexible bonding becomes preferred. We note the importance of weak hydrogen-bonding interactions for determining the stability of competing polymorphs has been previously observed experimentally in organic crystal systems and in lithium tartrate crystals [50].

In conclusion, we have studied the origins of vibrational entropy differences in hybrid-perovskite materials, by applying lattice dynamics calculations based on quantum mechanical forces. Our analysis allows us to quantify the contribution of vibrational entropy to total energies and demonstrate its crucial role in determining the stable polymorph. It is clear that vibrational entropy will always be an important consideration when predicting the preferred structure of hybrid organic-inorganic perovskite materials. We provide a theoretical basis for the observation that, in hybrid organic-inorganic materials, the materials favor structures that maximize the number of soft intermolecular interactions as the temperature rises. We demonstrated that the contribution of vibrational entropy can be quantitatively assessed and analyzed from lattice dynamics calculations even for soft hybrid organic-inorganic frameworks, which allows for the development of more general principles for understanding phase stability and transformations.

We acknowledge membership of the U.K.'s HPC Materials Chemistry Consortium (EPSRC EP/L000202) and access to computational resources through PRACE. A.W. acknowledges support from the Royal Society for a University Research Fellowship and K.T.B. is funded by EPSRC (EP/M009580/1 and EP/J017361/1). G.K. acknowledges support as the holder of a DFG fellowship (KI1870). G.K. and A.K.C. gratefully thank the Ras Al Khaimah Center for Advanced Materials for financial support. Data analysis scripts used to generate Figs. 2–4, the optimized structures, and data from the phonon calculations are available online, free of charge, from https://github.com/WMD-group/Phonons.

[1] V. M. Goldschmidt, J. Chem. Soc., 655 (1937).
[2] L. Pauling, J. Am. Chem. Soc. **51**, 1010 (1929).
[3] J. B. Goodenough, J. Phys. Chem. Solids **6**, 287 (1958).
[4] J. Kanamori, J. Phys. Chem. Solids **10**, 87 (1959).
[5] R. G. Pearson, J. Am. Chem. Soc. **85**, 3533 (1963).
[6] D. G. Pettifor, J. Phys.: Condens. Matter **15**, V13 (2003).
[7] K. F. Garrity, K. M. Rabe, and D. Vanderbilt, Phys. Rev. Lett. **112**, 127601 (2014).
[8] N. A. Benedek and C. J. Fennie, Phys. Rev. Lett. **106**, 107204 (2011).

[9] J. M. Rondinelli, M. Stengel, and N. A. Spaldin, Nat. Nanotechnol. **3**, 46 (2008).
[10] A. Jain, S. P. Ong, G. Hautier, W. Chen, W. D. Richards, S. Dacek, S. Cholia, D. Gunter, D. Skinner, G. Ceder, and K. A. Persson, APL Mater. **1**, 011002 (2013).
[11] L. M. Ghiringhelli, J. Vybiral, S. V. Levchenko, C. Draxl, and M. Scheffler, Phys. Rev. Lett. **114**, 105503 (2015).
[12] H. Li, M. Eddaoudi, M. O'Keeffe, and O. M. Yaghi, Nature (London) **402**, 276 (1999).
[13] T. Yildirim and M. R. Hartman, Phys. Rev. Lett. **95**, 215504 (2005).
[14] R. I. Thomson, P. Jain, A. K. Cheetham, and M. A. Carpenter, Phys. Rev. B **86**, 214304 (2012).
[15] A. Stroppa, P. Barone, P. Jain, J. M. Perez-Mato, and S. Picozzi, Adv. Mater. **25**, 2284 (2013).
[16] K. T. Butler, C. H. Hendon, and A. Walsh, J. Am. Chem. Soc. **136**, 2703 (2014).
[17] J. M. Frost, K. T. Butler, F. Brivio, C. H. Hendon, M. van Schilfgaarde, and A. Walsh, Nano Lett. **14**, 2584 (2014).
[18] H. Zhou, Q. Chen, G. Li, S. Luo, T.-b. Song, H.-S. Duan, Z. Hong, J. You, Y. Liu, and Y. Yang, Science **345**, 542 (2014).
[19] J. Li and P. M. Haney, Phys. Rev. B **93**, 155432 (2016).
[20] K. T. Butler, Y. Kumagai, F. Oba, and A. Walsh, J. Mater. Chem. C **4**, 1149 (2016).
[21] P. Horcajada, C. Serre, D. Grosso, C. Boissière, S. Perruchas, C. Sanchez, and G. Férey, Adv. Mater. **21**, 1931 (2009).
[22] E. Redel, Z. Wang, S. Walheim, J. Liu, H. Gliemann, and C. Wöll, Appl. Phys. Lett. **103**, 091903 (2013).
[23] W. Li, Z. Zhang, E. G. Bithell, A. S. Batsanov, P. T. Barton, P. J. Saines, P. Jain, C. J. Howard, M. A. Carpenter, and A. K. Cheetham, Acta Mater. **61**, 4928 (2013).
[24] K. L. Svane, P. J. Saines, and A. Walsh, J. Mater. Chem. C **3**, 11076 (2015).
[25] G. Kieslich, S. Sun, and A. K. Cheetham, Chem. Sci. **5**, 4712 (2014).
[26] W. Travis, E. N. K. Glover, H. Bronstein, D. O. Scanlon, and R. Palgrave, Chem. Sci. **7**, 4548 (2016).
[27] K. A. Muller, W. Berlinger, and E. Tosatti, Z. Phys. **84**, 277 (1991).
[28] U. V. Waghmare and K. M. Rabe, Phys. Rev. B **55**, 6161 (1997).
[29] E. A. Stern, Phys. Rev. Lett. **93**, 037601 (2004).
[30] Y. Qi, S. Liu, I. Grinberg, and A. M. Rappe, Phys. Rev. B **94**, 134308 (2016).
[31] M. S. Senn, D. A. Keen, T. C. A. Lucas, J. A. Hriljac, and A. L. Goodwin, Phys. Rev. Lett. **116**, 207602 (2016).
[32] K. T. Butler, A. Walsh, A. K. Cheetham, and G. Kieslich, Chem. Sci. **7**, 6316 (2016).
[33] H. D. Duncan, M. T. Dove, D. A. Keen, and A. E. Phillips, Dalton Trans. **45**, 4380 (2016).
[34] N. Onoda-Yamamuro, Physico-chemical study of some perovskite-type methylammonium trihalometallates, Ph.D. thesis, Osaka University, 1992.
[35] M. Habgood, R. Grau-Crespo, and S. L. Price, Phys. Chem. Chem. Phys. **13**, 9590 (2011).
[36] C. Caetano, K. T. Butler, and A. Walsh, Phys. Rev. B **93**, 144205 (2016).
[37] G. Kieslich, S. Kumagai, K. T. Butler, T. Okamura, C. H. Hendon, S. Sun, M. Yamashita, A. Walsh, and A. K. Cheetham, Chem. Commun. **51**, 15538 (2015).
[38] A. M. Walker, B. Civalleri, B. Slater, C. Mellot-Draznieks, F. Corà, C. M. Zicovich-Wilson, G. Romá-Pérez, J. M. Soler, and J. D. Gale, Angew. Chem. Int. Ed. **49**, 7501 (2010).
[39] C. Yi, J. Luo, S. Meloni, A. Boziki, N. Ashari-Astani, C. Gratzel, S. M. Zakeeruddin, U. Rothlisberger, and M. Gratzel, Energy Environ. Sci. **9**, 656 (2016).
[40] G. Kieslich, A. C. Forse, S. Sun, K. T. Butler, S. Kumagai, Y. Wu, M. R. Warren, A. Walsh, C. P. Grey, and A. K. Cheetham, Chem. Mater. **28**, 312 (2016).
[41] M. T. Weller, O. J. Weber, P. F. Henry, A. M. Di Pumpo, and T. C. Hansen, Chem. Commun. **51**, 4180 (2015).
[42] F. Brivio, J. M. Frost, J. M. Skelton, A. J. Jackson, O. J. Weber, M. T. Weller, A. R. Goñi, A. M. A. Leguy, P. R. F. Barnes, and A. Walsh, Phys. Rev. B **92**, 144308 (2015).
[43] K. T. Møller, M. B. Ley, P. Schouwink, R. Černý, and T. R. Jensen, Dalton Trans. **45**, 831 (2016).
[44] J. P. Perdew, A. Ruzsinszky, G. I. Csonka, O. A. Vydrov, G. E. Scuseria, L. A. Constantin, X. Zhou, and K. Burke, Phys. Rev. Lett. **100**, 136406 (2008).
[45] G. Kresse and J. Hafner, Phys. Rev. B **47**, 558 (1993).
[46] P. E. Blöchl, Phys. Rev. B **50**, 17953 (1994).
[47] J. Moreno and J. M. Soler, Phys. Rev. B **45**, 13891 (1992).
[48] A. Togo and I. Tanaka, Scr. Mater. **108**, 1 (2015).
[49] See Supplemental Material at http://link.aps.org/supplemental/10.1103/PhysRevB.94.180103 for the SI we present data showing the temperature evolution of how much regions of the phonon spectrum contribute to the vibrational entropy of the four systems.
[50] H. H.-M. Yeung and A. K. Cheetham, Dalton Trans. **43**, 95 (2014).